Editors' Suggestion

Flexible Readout and Unconditional Reset for Superconducting Multiqubit Processors with Tunable Purcell Filters

Yong-Xi Xiao,[1,2,*] Da'er Feng,[1,2,*] Xu-Yang Gu,[1,2] Gui-Han Liang,[1,2] Ming-Chuan Wang,[1,2] Zhen-Yu Peng,[1,2] Bing-Jie Chen,[1,2] Yu Yan,[1,2] Zheng-Yang Mei,[1,2] Si-Lu Zhao,[1,2] Yi-Zhou Bu,[1,2] Cheng-Lin Deng,[1,2] Kai Yang,[1,2] Ye Tian,[1] Xiaohui Song,[1,2] Dongning Zheng,[1,2,3,4] Yu-Xiang Zhang,[1,2] Yun-Hao Shi,[1] Zhongcheng Xiang,[1,2,3,4,†] Kai Xu,[1,2,3,4,5,‡] and Heng Fan[1,2,3,4,5,§]

[1]*Beijing National Laboratory for Condensed Matter Physics, Institute of Physics, Chinese Academy of Sciences, Beijing 100190, China*
[2]*School of Physics, University of Chinese Academy of Sciences, Beijing 100049, China*
[3]*Beijing Academy of Quantum Information Sciences, Beijing 100193, China*
[4]*Hefei National Laboratory, Hefei 230088, China*
[5]*Songshan Lake Materials Laboratory, Dongguan 523808, Guangdong, China*

(Received 17 July 2025; accepted 16 January 2026; published 17 February 2026)

Achieving high-fidelity qubit readout and reset while maintaining qubit coherence is crucial for quantum error correction and advanced quantum algorithms. Here, we design and experimentally demonstrate a scalable architecture based on frequency-tunable nonlinear Purcell filters, which enables flexible readout and rapid unconditional reset of multiple superconducting qubits. Our readout protocol dynamically adjusts the effective linewidth of the readout resonator through a tunable Purcell filter, optimizing the signal-to-noise ratio during measurement while suppressing photon noise during idle periods. Combined with a multilevel readout protocol, we achieve the highest readout fidelity of 99.3% without any quantum-limited amplifier, even with a small dispersive shift. Moreover, by leveraging a reset channel formed via the adjacent coupling between the filter and the coupler, we realize unconditional qubit reset of both leakage-induced $|2\rangle$ and $|1\rangle$ states within 200 ns and reset of the $|1\rangle$ state alone within 75 ns, with error rates $\leq 1\%$. The filter also mitigates both photon-induced dephasing and the Purcell effect, thereby preserving qubit coherence. This scalable Purcell filter architecture shows exceptional performance in qubit readout, reset, and protection, marking it as a promising hardware component for advancing fault-tolerant quantum computing systems.

DOI: 10.1103/vwrv-x1kr

Superconducting qubits have emerged as a leading platform for scalable, fault-tolerant quantum computation, driven by breakthroughs in coherence time, device integration, and control fidelity [1–4]. Recent advances have paved the way for large-scale quantum information processing, enabling demonstrations in quantum simulation and error correction [5–9]. As these applications grow in complexity, there is an increasing need for simultaneous improvements in qubit readout [10–13] and reset [14–17] to support high-fidelity and multilayer quantum operations.

Balancing high readout fidelity with qubit protection remains a central challenge in dispersive readout of superconducting qubits [18–22]. While fixed-frequency linear Purcell filters improve signal-to-noise ratio (SNR) and suppress the Purcell effect [10,20–25], they cannot fully mitigate photon-noise-induced dephasing. Recent demonstrations of nonlinear Purcell filters on single-qubit devices [26] have enabled photon-noise-tolerant readout, but rely on large dispersive shifts and remain unverified for scalability. Meanwhile, prior multiqubit implementations of high-fidelity readout typically depend on quantum-limited amplifiers such as Josephson parametric amplifiers or traveling-wave parametric amplifiers to achieve sub-1% readout error [27,28].

In this Letter, we present a scalable architecture of frequency-tunable nonlinear Purcell filters integrated into a superconducting multiqubit processor. By dynamically adjusting the effective linewidth of readout resonators through filter tuning, we optimize SNR for qubit state discrimination while suppressing photon noise during idle periods. Critically, this approach achieves 99.3% readout fidelity without requiring a quantum-limited amplifier, surpassing prior multiqubit benchmarks under comparable conditions. Our design operates with a small dispersive shift, enabling compatibility with compact, low-noise architectures.

Additionally, qubit reset capable of mitigating leakage errors is crucial for quantum error correction [29,30]. Thus, we experimentally implement a coupler-assisted qubit reset

*These authors contributed equally to this work.
†Contact author: zcxiang@iphy.ac.cn
‡Contact author: kaixu@iphy.ac.cn
§Contact author: hfan@iphy.ac.cn

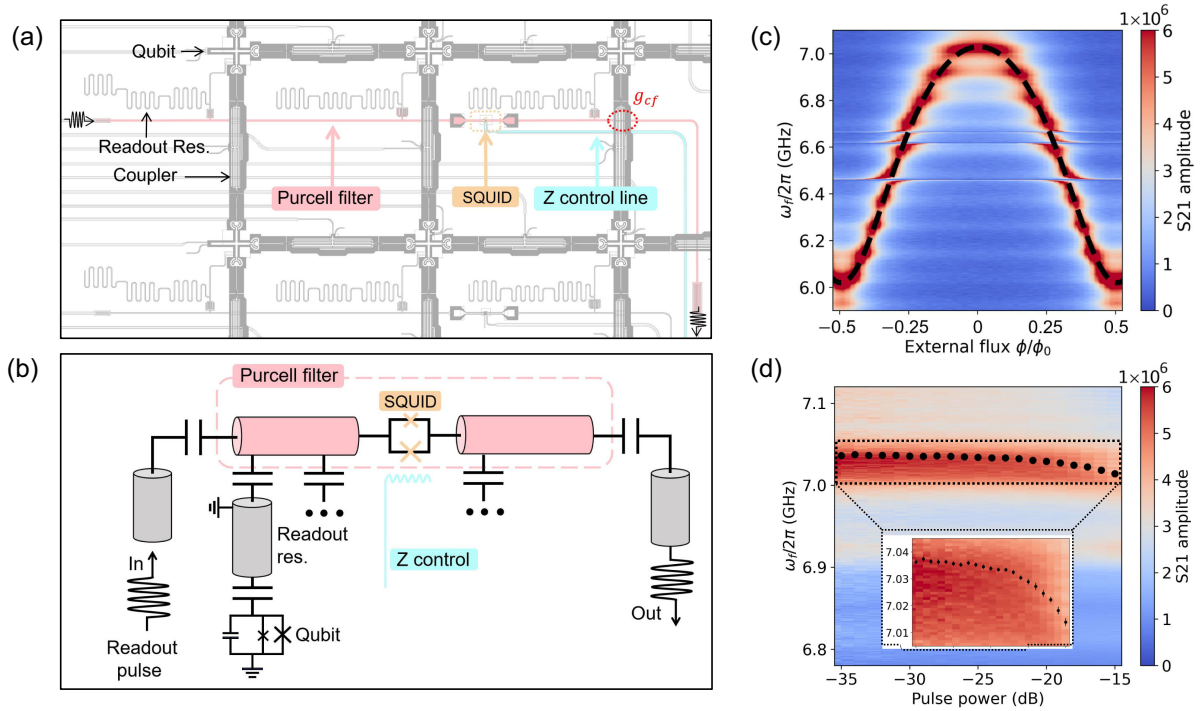

FIG. 1. Tunable Purcell filter integrated in a flip-chip quantum processor. (a) Filter-related structure. The filter (pink) consists of a half-wavelength resonator with open-ended capacitance coupling to the transmission line. The midpoint of the filter is integrated with a SQUID (orange) containing two Josephson junctions, of which the flux is modulated by the Z control line (blue). Each filter is shared by three readout resonators for qubit readout and coupled with couplers (circled in red) for qubit reset. (b) Distributed-element circuit model of the relevant device section with color coding matching (a). The ellipses denote other resonator-qubit systems and couplers capacitively coupled to the filter. (c) The variation of $S21$ amplitude under different external flux applied to the SQUID. Black dashed curve indicates fitted resonance frequencies of filter passbands. ϕ_0 is the magnetic flux quantum. (d) Power-dependent Kerr nonlinearity effect on the filter passband frequency. Black markers represent fitted resonance frequencies at the passband peaks.

protocol that utilizes the filter as a fast dissipation channel. This also demonstrates the functional versatility of our tunable Purcell filter. Our method achieves unconditional reset of leakage-induced $|2\rangle$ and $|1\rangle$ within 200 ns, while reset of $|1\rangle$ alone completes in just 75 ns, with error rates $\leq 1\%$. Compared to existing schemes that utilize readout resonators for dissipation [31,32], our approach significantly shortens reset time and minimizes crosstalk in multiqubit systems.

Our experiment employs a flip-chip superconducting quantum processor [4,33], interconnected via indium bump bonding. The device consists of aluminum-based coplanar waveguide circuits fabricated on sapphire substrates. The top chip contains 24 qubits, 38 couplers, and 8 superconducting quantum interference devices (SQUIDs) dedicated to filters, while the bottom chip serves as the wiring layer housing readout resonators, the main bodies of filters, and associated transmission lines. As shown in Figs. 1(a) and 1(b), each tunable Purcell filter is parametrically coupled to three readout resonators via capacitance. A filter comprises a nonlinear structure, based on a $\lambda/2$ cavity with open ends capacitively coupled with transmission line, incorporating a SQUID (composed of two Josephson junctions in parallel) at its midpoint. Note that the Josephson junctions of a filter are located on the top layer and are connected to the geometric cavity on the bottom layer through indium bumps. This design offers the advantage of enabling simultaneous fabrication of the Josephson junctions of filters, qubits, and couplers, thereby simplifying the fabrication process. Inputting dc signals through the Z-control line generates flux bias to tune the filter frequency from 6.02 to 7.06 GHz [Fig. 1(c)]. The power-dependent Kerr nonlinearity effect is another reason for frequency changes. The nonlinear frequency shift remains negligible at low power levels [Fig. 1(d)] because of a small anharmonicity of $\alpha_f/2\pi = 4.47$ MHz. The frequency of this filter can be dynamically tuned through SQUID flux and readout pulse amplitude. This enables real-time optimization of effective linewidth κ_{eff} of readout resonators through the filter, aiming to achieve optimal readout conditions (typically targeting $2\chi = \kappa_{\text{eff}}$, where 2χ is the dispersive shift). This addresses the limitation of fixed-bandwidth linear filters, where fabrication-induced frequency deviations may cause $2\chi \neq \kappa_{\text{eff}}$. Furthermore, the tunable Purcell filter passband frequency expands the frequency allocation range of readout resonators on a single feedline, thereby mitigating frequency crowding in multiqubit readout.

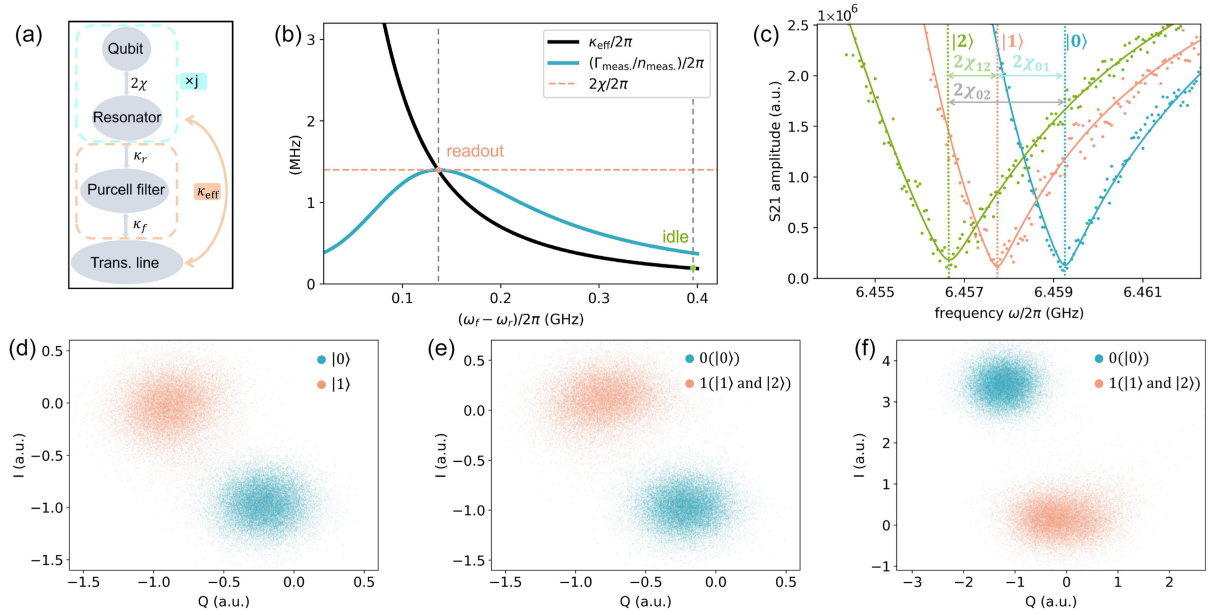

FIG. 2. Experimental demonstration of flexible readout. (a) Schematic of the qubit readout system with tunable Purcell filters. The tunable Purcell filter functions to adjust κ_{eff}. Each filter is coupled with j resonators ($j = 3$ here). (b) Variation curves of κ_{eff} and $\Gamma_{\mathrm{meas}}/n_{\mathrm{meas}}$ versus frequency difference between the filter and readout resonator. The filter frequency resides at a point maximizing $\Gamma_{\mathrm{meas}}/n_{\mathrm{meas}}$ (where $\kappa_{\mathrm{eff}} = 2\chi$) during readout, while at a lower point during idle time. (c) The fitted dressed-state frequencies of the readout resonator with different qubit states. To maximize state distinguishability when distinguishing qubit states $|i\rangle$ and $|j\rangle$, the effective linewidth is set to $\kappa_{\mathrm{eff}} = 2\chi_{ij}$. (d)–(f) Typical data of IQ raw data: (d) 500 ns readout with direct measurement. (e) 500 ns readout with pre-π_{12}-pulse, mitigating qubit decoherence effects compared to (d). (f) 1077 ns readout duration with pre-π_{12}-pulse, achieving enhanced SNR over (e) and 99.3% readout fidelity.

The SNR represents a crucial metric in high-fidelity dispersive readout [11,13], scaling with $\mathrm{SNR}^2 \propto \eta\kappa\bar{n}|\sin(2\theta)|^2 t$, with $|\sin(2\theta)| = \chi\kappa/(\chi^2 + \kappa^2/4)$, where κ denotes the linewidth of the readout resonator, η is the quantum efficiency, $\bar{n}$ is the average photon number, and t is the readout time. $|\sin(2\theta)|^2 = 1$ is satisfied when $\kappa = 2\chi$. Figure 2(a) illustrates the readout scheme incorporating a tunable Purcell filter, of which the role manifests in modifying κ_{eff} to optimize SNR. Filter frequency modulation induces corresponding changes in κ_{eff}, as shown in Fig. 2(b). The measurement-induced dephasing rate Γ_{meas} is defined by $\Gamma_{\mathrm{meas}}/n_{\mathrm{meas}} = 2\chi|\sin(2\theta)|$, where n_{meas} is the average photon number in the readout resonator; Γ_{meas} is the upper limit of measurement rate [34]. During active readout operations, the filter frequency aligns with the $\kappa_{\mathrm{eff}} = 2\chi$ configuration to maximize SNR and $\Gamma_{\mathrm{meas}}/n_{\mathrm{meas}}$ with a given 2χ. During idle periods, the filter frequency remains at a low-dephasing-rate operating point (idle point, where $\kappa \neq 2\chi$), enabling enhanced suppression of photon noise compared to conventional fixed-frequency filters. To verify the tunable Purcell filter's suppression effect on photon noise, we intentionally inject white Gaussian noise into the readout transmission line and measure the dephasing rate of a qubit, as shown in Fig. 3. Furthermore, the idle point maintains greater detuning between filter and qubit, providing additional suppression of Purcell effects.

Notably, the dispersive shift 2χ of dressed states under different qubit states is not a fixed parameter [Fig. 2(c)]. This observation highlights important considerations: while direct measurements of qubit $|0\rangle$-$|1\rangle$ remain standard practice, contemporary protocols also employ π_{12}-pulse-assisted $|0\rangle$-$|2\rangle$ readout [61,62]. $|0\rangle$-$|2\rangle$ readout means implementing a nondiscriminating readout between $|1\rangle$ and $|2\rangle$ states, wherein: (i) All results measured in either $|1\rangle$ or $|2\rangle$ are registered as logical "1." (ii) Only $|0\rangle$ measurements yield logical "0" outputs. The logical 0 or 1 is the single-shot measurement result. The filter provides adaptable κ_{eff} values to accommodate various readout requirements. For instance, Figs. 2(d) and 2(e) present in-phase and quadrature (IQ) raw data for $|0\rangle$-$|1\rangle$ and $|0\rangle$-$|2\rangle$ readouts with 500 ns integration times, achieving SNR of 4.6 and 4.9, respectively. The $|0\rangle$-$|2\rangle$ readout mitigates T_1-limited fidelity constraints, enabling extension of integration time to 1077 ns [Fig. 2(f)] with SNR improvement to 6.4 and a readout fidelity $\geq 99.3\%$. Here readout fidelity is defined as $F = [P(0|0) + P(1|1)]/2$, where $P(a|b)$ denotes the probability that qubit is prepared in $|b\rangle$ state and then measured in $|a\rangle$ state. SNR is calculated with $\mathrm{SNR} = 2|m_0 - m_1|/(\sigma_0 + \sigma_1)$ [11,25], where $m_{0(1)}$ and $\sigma_{0(1)}$ are the mean and standard deviation of the Gaussian fits to IQ data of $|0\rangle(|1\rangle)$. Notably, the extended readout duration originates from the weak coupling design between readout resonators and qubits,

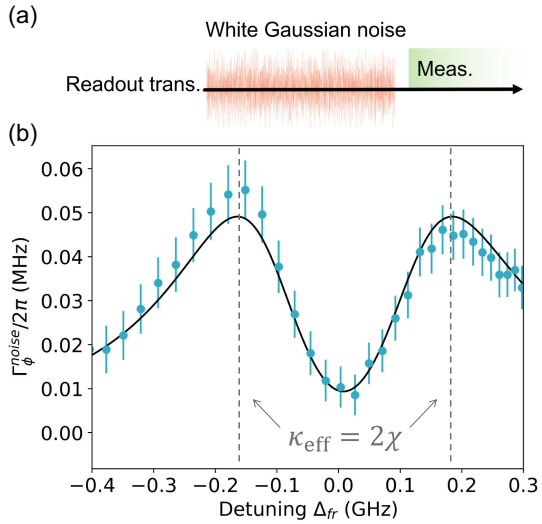

FIG. 3. Evaluation of the noise tolerance. (a) Pulse sequence. The qubit T_2 is measured while applying white Gaussian noise through the readout transmission line. (b) Qubit dephasing rate versus detuning. The dephasing rate $\Gamma_{\rm meas}$ reaches a maximum when the detuning Δ_{fr} satisfies $\kappa_{\rm eff} = 2\chi$. The black curve shows the fit using a photon-noise-induced dephasing model (see Supplemental Material [35] for details).

implemented to preserve qubit coherence for complex multiqubit gate operations. Each IQ distribution derives from 30 000 single-shot measurements. The increased leakage error potentially introduced by $|0\rangle$-$|2\rangle$ readout can be mitigated by the reset scheme proposed later in this Letter. Multiplexed readout and more details are shown in Supplemental Material [35].

Furthermore, we introduce a coupler-assisted qubit reset protocol leveraging the Purcell filter as a dissipation channel. Categorized into active (conditional) [63,64] and passive (unconditional) [31,65,66] approaches based on whether qubit state information is required, rapid qubit reset techniques could be applied to various quantum information processing tasks, especially the quantum error correction codes [67]. While introducing additional decay channel risks complicating multiqubit integration, the coupler-assisted reset offers a hardware-efficient solution [31,32]. However, existing schemes utilize the readout resonator for dissipation, whose rate is significantly lower than that of the filter. Employing the filter would further reduce the reset time and the error rate. In our flip-chip processor, qubits and couplers are placed on one layer, while transmission lines and Purcell filters are located on another layer [3,5,9]. Inevitably, filters traverse above couplers or qubits as shown in Fig. 1(a). The former results in a coupling strength $g_{\rm cf}$ between filters and couplers. We ingeniously exploit this coupling to facilitate qubit reset. Crucially, the filter and readout resonators remain detuned throughout the process (filter, 7.0 GHz; readout resonators, 6.4–6.6 GHz in this experiment), effectively suppressing photon leakage into the readout resonators. This detuning strategy requires a frequency-tunable Purcell filter, as fixed-frequency filters must operate near the readout resonator frequency to maintain measurement fidelity, and the detuning avoids keeping the coupler at the readout resonator frequency, which would trigger complex multibody processes.

As illustrated in Fig. 4(a), our reset protocol comprises three sequential steps. Step 1 involves adiabatic state swap between the qubit and coupler. The resonance between the coupler and the target qubit introduces nonzero coupling between the target qubit and another qubit connected via the same coupler. To ensure exclusive photon transfer to the coupler, the frequencies of these two qubits are intentionally detuned by 800 MHz here. Step 2 utilizes the capacitive coupling mentioned above to perform adiabatic swap between the coupler and the filter. Step 3 involves rapid photon dissipation from the filter, enabled by its leakage rate (linewidth) $\kappa_f/2\pi = 150$ MHz. It is noted that the linewidth of the filter is approximately 100 times larger than that of the readout resonator. Thus, step 3 executes concurrently within operational time frame of step 2, requiring virtually no additional time. Especially, the coupler frequency starts below the target qubit frequency (and above the neighboring), sweeps through it, and continues ascending to the filter frequency to suppress Landau-Zener-Stückelberg interference [68], which could otherwise degrade reset fidelity.

To validate the unconditional nature and leakage-error mitigation capability of this reset protocol, we conduct the experimental demonstration outlined in Fig. 4(b). First, the qubit is prepared in varying excited states by applying π_{01} pulses and π_{12} fractional pulses of different amplitudes ($A\pi_{12}$ with A from 0 to 1). Then a standardized reset operation (waveform details are shown in Supplemental Material [35]) is executed by adjusting the coupler flux bias. State preparation is repeated for m rounds. After each round, reset operations would be executed for n cycles. The result of a preparation round with $\pi_{01} + A\pi_{12}$ and a reset cycle is shown in Fig. 4(c). The qubit-coupler swap and coupler-filter swap are completed within 30 and 170 ns, respectively, yielding a total reset within 200 ns. Immediate postreset qubit measurements reveal the population of excited state below 1.2% across all initial states. After accounting for a 0.45% ground-state readout error (attributed to state discrimination limitation and natural thermal excitation), the unconditional reset error per cycle is inferred to below 1%.

Further investigation of consecutive multicycle reset operations after a round of state preparation with $\pi_{01} + \pi_{12}$, as shown in Fig. 4(d), demonstrates progressive reduction of residual excitations with increasing reset cycles, converging to natural thermal excitation levels (quantified by a deviation less than 0.1% from ground-state readout error line) after three cycles (600 ns). Critically, multiple reset cycles do not accumulate errors via photon recapture, confirming effective dissipation through the filter. Consider the following scenario: the qubit state is repeatedly prepared for m rounds at

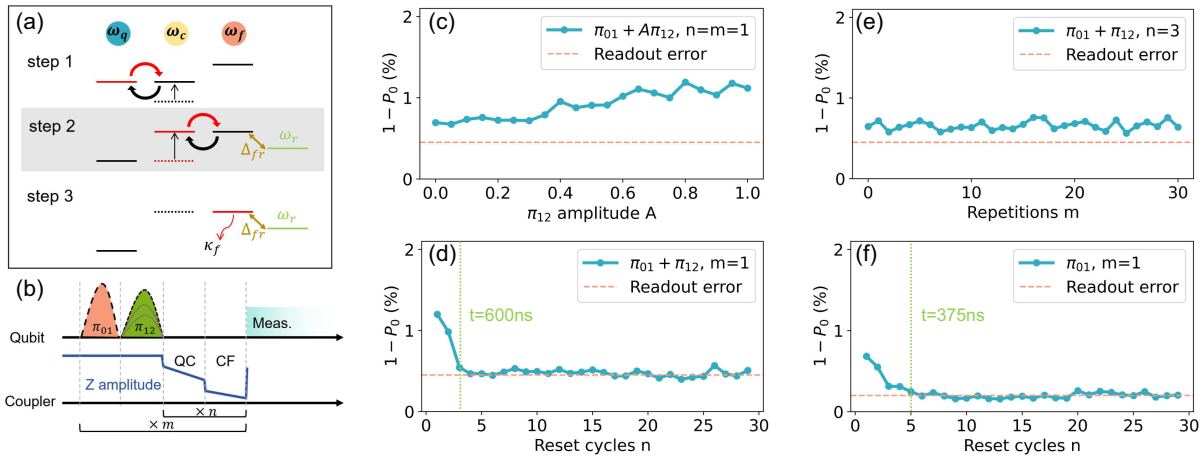

FIG. 4. Experimental demonstration of unconditional qubit reset. (a) Reset protocol. Step 1: Qubit-coupler (QC) swap. Step 2: Coupler-filter (CF) swap. Step 3: Dissipation of excitation into the environment via the Purcell filter. Steps 2 and 3 occur concurrently, with the filter detuned from the readout resonators to avoid crosstalk. (b) Pulse sequence for state preparation, reset, and measurement. (c)–(f) Residual qubit excitation after reset, quantified by the measured $|0\rangle$ state population P_0. (c) Single reset cycle (200 ns), preparing initial state with π_{01} and $A\pi_{12}$, where $0 \leq A \leq 1$. (d) Multiple reset cycles, with state preparation using π_{01} and π_{12}. (e) Repeated state preparation (for m rounds) followed by three reset cycles each time. (f) Multiple reset cycles with initialization using only the full π_{01} pulse.

intervals of 1 ms, and the cycle of resets after each state preparation is $n = 3$. As shown in Fig. 4(d), the residual thermal excitation does not increase with the growth of m, which indicates that short-time multiple excitations and resets of the qubit is supported. In other words, this dissipation channel can be rapidly reused. When exclusively considering $|1\rangle$ excitation, we employ square pulse for QC and CF swap. The single-cycle reset operation can be optimized to complete within 75 ns (4.5 and 70 ns for qubit-coupler and coupler-filter swap) with a error rate below 1%, and the residual thermal excitation decreases and converges to the natural scenario after the fifth cycle (375 ns), with a deviation from readout error line below 0.1%. Each data point in Figs. 4(c)–4(f) is derived from 30 000 repetitions of single-shot measurements. The readout error line in Fig. 4(f) differs from those in other figures due to different readout parameters. Comparing with recent reports on the unconditional reset for quantum error correction [32,67,69], the time cost and error rate of our protocol are smaller. Therefore, our reset protocol has the potential to be applied in complex algorithms such as quantum error correction, where the reset operations are executed frequently. The discussion on leakage reduction is provided in Supplemental Material [35].

In conclusion, we present a scalable structure of tunable-frequency nonlinear Purcell filters for superconducting multiqubit processors. Based on this structure, we implement a flexible readout protocol featuring the κ_{eff}-tuning capability of filters to maximize SNR during readout and suppress photon noise during idle time. Without a quantum-limited amplifier, we achieve the highest readout fidelity of 99.3% with a small dispersive shift of 1.4 MHz. By leveraging the coupling between couplers and filters in a flip-chip architecture, we propose an unconditional qubit reset protocol. This protocol eliminates both leakage-induced $|2\rangle$ and $|1\rangle$ states with a rate that exceeds natural qubit relaxation by a factor of 10^3. Thus, this tunable-frequency nonlinear Purcell filter structure represents a highly potential auxiliary hardware component to advance the development of fault-tolerant quantum computing systems. We provide the parameter calculation, experimental detail, and numerical analysis in Supplemental Material [35]. Future improvements may focus on extending the filter geometry by utilizing the frequency-tunable property in a $n\lambda/2$ resonator to read out more qubits. Since the reset time is primarily limited by the coupler-filter coupling strength g_{cf}, increasing g_{cf} could achieve faster reset operation.

Acknowledgments—This work is supported by the National Natural Science Foundation of China (Grants No. T2322030, No. T2121001, No. 92265207, No. 12122504, No. 12274142, No. 92365206, and No. 12104055), the Innovation Program for Quantum Science and Technology (Grant No. 2021ZD0301800), the Beijing Nova Program (No. 20220484121), and the China Postdoctoral Science Foundation (Grant No. GZB20240815). We acknowledge the support from the Synergetic Extreme Condition User Facility (SECUF).

Data availability—The data that support the findings of this article are not publicly available upon publication because it is not technically feasible and/or the cost of preparing, depositing, and hosting the data would be prohibitive within the terms of this research project. The data are available from the authors upon reasonable request.

[1] M. Kjaergaard, M. E. Schwartz, J. Braumüller, P. Krantz, J. I.-J. Wang, S. Gustavsson, and W. D. Oliver, Superconducting qubits: Current state of play, Annu. Rev. Condens. Matter Phys. **11**, 369 (2020).

[2] C. Wang *et al.*, Towards practical quantum computers: Transmon qubit with a lifetime approaching 0.5 milliseconds, npj Quantum Inf. **8**, 3 (2022).

[3] P. Zhang *et al.*, Emergence of steady quantum transport in a superconducting processor, Nat. Commun. **15**, 10115 (2024).

[4] G.-H. Liang *et al.*, Tunable-coupling architectures with capacitively connecting pads for large-scale superconducting multiqubit processors, Phys. Rev. Appl. **20**, 044028 (2023).

[5] Y. Zhao *et al.*, Realization of an error-correcting surface code with superconducting qubits, Phys. Rev. Lett. **129**, 030501 (2022).

[6] S. Krinner, N. Lacroix, A. Remm, A. Di Paolo, E. Genois, C. Leroux, C. Hellings, S. Lazar, F. Swiadek, J. Herrmann, G. J. Norris, C. K. Andersen, M. Mueller, A. Blais, C. Eichler, and A. Wallraff, Realizing repeated quantum error correction in a distance-three surface code, Nature (London) **605**, 669 (2022).

[7] C.-L. Deng *et al.*, High-order topological pumping on a superconducting quantum processor, Phys. Rev. Lett. **133**, 140402 (2024).

[8] Y.-Y. Wang *et al.*, Exploring Hilbert-space fragmentation on a superconducting processor, PRX Quantum **6**, 010325 (2025).

[9] Google Quantum AI and Collaborators, Quantum error correction below the surface code threshold, Nature (London) **638**, 920 (2025).

[10] D. Sank *et al.*, Measurement-induced state transitions in a superconducting qubit: Beyond the rotating wave approximation, Phys. Rev. Lett. **117**, 190503 (2016).

[11] A. Blais, A. L. Grimsmo, S. M. Girvin, and A. Wallraff, Circuit quantum electrodynamics, Rev. Mod. Phys. **93**, 025005 (2021).

[12] R. Shillito, A. Petrescu, J. Cohen, J. Beall, M. Hauru, M. Ganahl, A. G. Lewis, G. Vidal, and A. Blais, Dynamics of transmon ionization, Phys. Rev. Appl. **18**, 034031 (2022).

[13] Y. Ye, J. B. Kline, S. Chen, A. Yen, and K. P. O'Brien, Ultrafast superconducting qubit readout with the quarton coupler, Sci. Adv. **10**, eado9094 (2024).

[14] D. Egger, M. Werninghaus, M. Ganzhorn, G. Salis, A. Fuhrer, P. Müller, and S. Filipp, Pulsed reset protocol for fixed-frequency superconducting qubits, Phys. Rev. Appl. **10**, 044030 (2018).

[15] T. Yoshioka, H. Mukai, A. Tomonaga, S. Takada, Y. Okazaki, N.-H. Kaneko, S. Nakamura, and J.-S. Tsai, Active initialization experiment of a superconducting qubit using a quantum circuit refrigerator, Phys. Rev. Appl. **20**, 044077 (2023).

[16] V. Maurya, H. Zhang, D. Kowsari, A. Kuo, D. M. Hartsell, C. Miyamoto, J. Liu, S. Shanto, E. Vlachos, A. Zarassi, K. W. Murch, and E. M. Levenson-Falk, On-demand driven dissipation for cavity reset and cooling, PRX Quantum **5**, 020321 (2024).

[17] J. Ding, Y. Li, H. Wang, G. Xue, T. Su, C. Wang, W. Sun, F. Li, Y. Zhang, Y. Gao, J. Peng, Z. H. Jiang, Y. Yu, H. Yu, and F. Yan, Multipurpose architecture for fast reset and protective readout of superconducting qubits, Phys. Rev. Appl. **23**, 014012 (2025).

[18] A. Blais, R.-S. Huang, A. Wallraff, S. M. Girvin, and R. J. Schoelkopf, Cavity quantum electrodynamics for superconducting electrical circuits: An architecture for quantum computation, Phys. Rev. A **69**, 062320 (2004).

[19] J. Koch, T. M. Yu, J. Gambetta, A. A. Houck, D. I. Schuster, J. Majer, A. Blais, M. H. Devoret, S. M. Girvin, and R. J. Schoelkopf, Charge-insensitive qubit design derived from the Cooper pair box, Phys. Rev. A **76**, 042319 (2007).

[20] E. Jeffrey, D. Sank, J. Y. Mutus, T. C. White, J. Kelly, R. Barends, Y. Chen, Z. Chen, B. Chiaro, A. Dunsworth, A. Megrant, P. J. J. O'Malley, C. Neill, P. Roushan, A. Vainsencher, J. Wenner, A. N. Cleland, and J. M. Martinis, Fast accurate state measurement with superconducting qubits, Phys. Rev. Lett. **112**, 190504 (2014).

[21] T. Walter, P. Kurpiers, S. Gasparinetti, P. Magnard, A. Potočnik, Y. Salathé, M. Pechal, M. Mondal, M. Oppliger, C. Eichler, and A. Wallraff, Rapid high-fidelity single-shot dispersive readout of superconducting qubits, Phys. Rev. Appl. **7**, 054020 (2017).

[22] J. Heinsoo, C. K. Andersen, A. Remm, S. Krinner, T. Walter, Y. Salathé, S. Gasparinetti, J.-C. Besse, A. Potočnik, A. Wallraff, and C. Eichler, Rapid High-fidelity multiplexed readout of superconducting qubits, Phys. Rev. Appl. **10**, 034040 (2018).

[23] M. D. Reed, B. R. Johnson, A. A. Houck, L. DiCarlo, J. M. Chow, D. I. Schuster, L. Frunzio, and R. J. Schoelkopf, Fast reset and suppressing spontaneous emission of a superconducting qubit, Appl. Phys. Lett. **96**, 203110 (2010).

[24] M. Khezri, A. Opremcak, Z. Chen, K. C. Miao, M. McEwen, A. Bengtsson, T. White, O. Naaman, D. Sank, A. N. Korotkov, Y. Chen, and V. Smelyanskiy, Measurement-induced state transitions in a superconducting qubit: Within the rotating-wave approximation, Phys. Rev. Appl. **20**, 054008 (2023).

[25] P. A. Spring, L. Milanovic, Y. Sunada, S. Wang, A. F. van Loo, S. Tamate, and Y. Nakamura, Fast multiplexed superconducting-qubit readout with intrinsic purcell filtering using a multiconductor transmission line, PRX Quantum **6**, 020345 (2025).

[26] Y. Sunada, K. Yuki, Z. Wang, T. Miyamura, J. Ilves, K. Matsuura, P. A. Spring, S. Tamate, S. Kono, and Y. Nakamura, Photon-noise-tolerant dispersive readout of a superconducting qubit using a nonlinear purcell filter, PRX Quantum **5**, 010307 (2024).

[27] F. m. c. Swiadek, R. Shillito, P. Magnard, A. Remm, C. Hellings, N. Lacroix, Q. Ficheux, D. C. Zanuz, G. J. Norris, A. Blais, S. Krinner, and A. Wallraff, Enhancing dispersive readout of superconducting qubits through dynamic control of the dispersive shift: Experiment and theory, PRX Quantum **5**, 040326 (2024).

[28] A. Bengtsson, A. Opremcak, M. Khezri, D. Sank, A. Bourassa, K. J. Satzinger, S. Hong, C. Erickson, B. J. Lester, K. C. Miao, A. N. Korotkov, J. Kelly, Z. Chen, and P. V. Klimov, Model-based optimization of superconducting qubit readout, Phys. Rev. Lett. **132**, 100603 (2024).

[29] T. Wang, F. Wu, F. Wang, X. Ma, G. Zhang, J. Chen, H. Deng, R. Gao, R. Hu, L. Ma, Z. Song, T. Xia, M. Ying,

H. Zhan, H.-H. Zhao, and C. Deng, Efficient initialization of fluxonium qubits based on auxiliary energy levels, Phys. Rev. Lett. **132**, 230601 (2024).

[30] N. Lacroix, L. Hofele, A. Remm, O. Benhayoune-Khadraoui, A. McDonald, R. Shillito, S. Lazar, C. Hellings, F. m. c. Swiadek, D. Colao-Zanuz, A. Flasby, M. B. Panah, M. Kerschbaum, G. J. Norris, A. Blais, A. Wallraff, and S. Krinner, Fast flux-activated leakage reduction for superconducting quantum circuits, Phys. Rev. Lett. **134**, 120601 (2025).

[31] L. Chen *et al.*, Fast unconditional reset and leakage reduction in fixed-frequency transmon qubits, arXiv:2409.16748.

[32] X. Yang *et al.*, Coupler-assisted leakage reduction for scalable quantum error correction with superconducting qubits, Phys. Rev. Lett. **133**, 170601 (2024).

[33] Z.-H. Liu *et al.*, Prethermalization by random multipolar driving on a 78-Qubit superconducting processor, arXiv:2503.21553.

[34] A. A. Clerk, M. H. Devoret, S. M. Girvin, F. Marquardt, and R. J. Schoelkopf, Introduction to quantum noise, measurement, and amplification, Rev. Mod. Phys. **82**, 1155 (2010).

[35] See Supplemental Material at http://link.aps.org/supplemental/10.1103/vwrv-x1kr for additional information on the device parameters, readout optimization, reset experiment, numerical simulations, and discussions of scalability and crosstalk, which includes Refs. [36–60].

[36] Y. Sunada, S. Kono, J. Ilves, S. Tamate, T. Sugiyama, Y. Tabuchi, and Y. Nakamura, Fast readout and reset of a superconducting qubit coupled to a resonator with an intrinsic purcell filter, Phys. Rev. Appl. **17**, 044016 (2022).

[37] E. Boaknin, V. E. Manucharyan, S. Fissette, M. Metcalfe, L. Frunzio, R. Vijay, I. Siddiqi, A. Wallraff, R. J. Schoelkopf, and M. Devoret, Dispersive microwave bifurcation of a superconducting resonator cavity incorporating a Josephson junction, arXiv:cond-mat/0702445.

[38] F. Mallet, F. R. Ong, A. Palacios-Laloy, F. Nguyen, P. Bertet, D. Vion, and D. Esteve, Single-shot qubit readout in circuit quantum electrodynamics, Nat. Phys. **5**, 791 (2009).

[39] R. Vijay, M. H. Devoret, and I. Siddiqi, Invited review article: The Josephson bifurcation amplifier, Rev. Sci. Instrum. **80**, 111101 (2009).

[40] P. Krantz, M. Kjaergaard, F. Yan, T. P. Orlando, S. Gustavsson, and W. D. Oliver, A quantum engineer's guide to superconducting qubits, Appl. Phys. Rev. **6**, 021318 (2019).

[41] Z.-X. Man, Y.-J. Xia, and R. Lo Franco, Harnessing non-Markovian quantum memory by environmental coupling, Phys. Rev. A **92**, 012315 (2015).

[42] C. C. Bultink, B. Tarasinski, N. Haandbæk, S. Poletto, N. Haider, D. J. Michalak, A. Bruno, and L. DiCarlo, General method for extracting the quantum efficiency of dispersive qubit readout in circuit QED, Appl. Phys. Lett. **112**, 092601 (2018).

[43] E. A. Sete, J. M. Martinis, and A. N. Korotkov, Quantum theory of a bandpass purcell filter for qubit readout, Phys. Rev. A **92**, 012325 (2015).

[44] J. Choi, H. Hwang, and E. Kim, Measurement-induced bistability in the excited state of a transmon, Phys. Rev. Appl. **22**, 054069 (2024).

[45] T. Akiba, S. Sano, T. Yanase, T. Ohta, and M. Koyama, Optuna: A next-generation hyperparameter optimization framework, in *Proceedings of the 25th ACM SIGKDD International Conference on Knowledge Discovery & Data Mining*, KDD '19 (Association for Computing Machinery, New York, USA, 2019), pp. 2623–2631.

[46] T.-M. Li *et al.*, High-precision pulse calibration of tunable couplers for high-fidelity two-qubit gates in superconducting quantum processors, Phys. Rev. Appl. **23**, 024059 (2025).

[47] D. Sank, A. Opremcak, A. Bengtsson, M. Khezri, Z. Chen, O. Naaman, and A. Korotkov, System characterization of dispersive readout in superconducting qubits, Phys. Rev. Appl. **23**, 024055 (2025).

[48] H. Yan, X. Wu, A. Lingenfelter, Y. J. Joshi, G. Andersson, C. R. Conner, M.-H. Chou, J. Grebel, J. M. Miller, R. G. Povey, H. Qiao, A. A. Clerk, and A. N. Cleland, Broadband bandpass purcell filter for circuit quantum electrodynamics, Appl. Phys. Lett. **123**, 134001 (2023).

[49] F. Yan, P. Krantz, Y. Sung, M. Kjaergaard, D. L. Campbell, T. P. Orlando, S. Gustavsson, and W. D. Oliver, Tunable coupling scheme for implementing high-fidelity two-qubit gates, Phys. Rev. Appl. **10**, 054062 (2018).

[50] E. A. Sete, N. Didier, A. Q. Chen, S. Kulshreshtha, R. Manenti, and S. Poletto, Parametric-resonance entangling gates with a tunable coupler, Phys. Rev. Appl. **16**, 024050 (2021).

[51] X. Li *et al.*, Vacuum-gap transmon qubits realized using flip-chip technology, Appl. Phys. Lett. **119**, 184003 (2021).

[52] L. Chen *et al.*, Transmon qubit readout fidelity at the threshold for quantum error correction without a quantum-limited amplifier, npj Quantum Inf. **9**, 26 (2023).

[53] A. Gold, J. P. Paquette, A. Stockklauser, M. J. Reagor, M. S. Alam, A. Bestwick, N. Didier, A. Nersisyan, F. Oruc, A. Razavi, B. Scharmann, E. A. Sete, B. Sur, D. Venturelli, C. J. Winkleblack, F. Wudarski, M. Harburn, and C. Rigetti, Entanglement across separate silicon dies in a modular superconducting qubit device, npj Quantum Inf. **7**, 142 (2021).

[54] G. J. Norris, K. Dalton, D. C. Zanuz, A. Rommens, A. Flasby, M. B. Panah, F. Swiadek, C. Scarato, C. Hellings, J.-C. Besse, and A. Wallraff, Performance characterization of a multi-module quantum processor with static inter-chip couplers, arXiv:2503.12603.

[55] X. Wu, H. Yan, G. Andersson, A. Anferov, M.-H. Chou, C. R. Conner, J. Grebel, Y. J. Joshi, S. Li, J. M. Miller, R. G. Povey, H. Qiao, and A. N. Cleland, Modular quantum processor with an all-to-all reconfigurable router, Phys. Rev. X **14**, 041030 (2024).

[56] K. Dalton, J. Knörzer, F. Hoehne, Y. Song, A. Flasby, D. C. Zanuz, M. B. Panah, I. Besedin, J.-C. Besse, and A. Wallraff, Resource-efficient cross-platform verification with modular superconducting devices, PRX Quantum **6**, 040365 (2025).

[57] S. Ihssen, S. Geisert, G. Jauma, P. Winkel, M. Spiecker, N. Zapata, N. Gosling, P. Paluch, M. Pino, T. Reisinger, W. Wernsdorfer, J. J. Garcia-Ripoll, and I. M. Pop, Low cross-talk modular flip-chip architecture for coupled superconducting qubits, Appl. Phys. Lett. **126**, 134003 (2025).

[58] M. Field, A. Q. Chen, B. Scharmann, E. A. Sete, F. Oruc, K. Vu, V. Kosenko, J. Y. Mutus, S. Poletto, and A. Bestwick, Modular superconducting-qubit architecture with a multichip tunable coupler, Phys. Rev. Appl. **21**, 054063 (2024).

[59] Y.-H. Shi, R.-Q. Yang, Z. Xiang, Z.-Y. Ge, H. Li, Y.-Y. Wang, K. Huang, Y. Tian, X. Song, D. Zheng, K. Xu, R.-G. Cai, and H. Fan, Quantum simulation of Hawking radiation and curved spacetime with a superconducting on-chip black hole, Nat. Commun. **14**, 3263 (2023).

[60] H. Li, Y.-Y. Wang, Y.-H. Shi, K. Huang, X. Song, G.-H. Liang, Z.-Y. Mei, B. Zhou, H. Zhang, J.-C. Zhang, S. Chen, S. P. Zhao, Y. Tian, Z.-Y. Yang, Z. Xiang, K. Xu, D. Zheng, and H. Fan, Observation of critical phase transition in a generalized Aubry-Andre-Harper model with superconducting circuits, npj Quantum Inf. **9**, 40 (2023).

[61] S. S. Elder, C. S. Wang, P. Reinhold, C. T. Hann, K. S. Chou, B. J. Lester, S. Rosenblum, L. Frunzio, L. Jiang, and R. J. Schoelkopf, High-fidelity measurement of qubits encoded in multilevel superconducting circuits, Phys. Rev. X **10**, 011001 (2020).

[62] D. Gao *et al.*, Establishing a new benchmark in quantum computational advantage with 105-qubit zuchongzhi 3.0 processor, Phys. Rev. Lett. **134**, 090601 (2025).

[63] D. Ristè, J. G. van Leeuwen, H.-S. Ku, K. W. Lehnert, and L. DiCarlo, Initialization by measurement of a superconducting quantum bit circuit, Phys. Rev. Lett. **109**, 050507 (2012).

[64] M. S. Moreira, G. G. Guerreschi, W. Vlothuizen, J. F. Marques, J. van Straten, S. P. Premaratne, X. Zou, H. Ali, N. Muthusubramanian, C. Zachariadis, J. van Someren, M. Beekman, N. Haider, A. Bruno, C. G. Almudever, A. Y. Matsuura, and L. DiCarlo, Realization of a quantum neural network using repeat-until-success circuits in a superconducting quantum processor, npj Quantum Inf. **9**, 118 (2023).

[65] Y. Zhou, Z. Zhang, Z. Yin, S. Huai, X. Gu, X. Xu, J. Allcock, F. Liu, G. Xi, Q. Yu, H. Zhang, M. Zhang, H. Li, X. Song, Z. Wang, D. Zheng, S. An, Y. Zheng, and S. Zhang, Rapid and unconditional parametric reset protocol for tunable superconducting qubits, Nat. Commun. **12**, 5924 (2021).

[66] P. Magnard, P. Kurpiers, B. Royer, T. Walter, J.-C. Besse, S. Gasparinetti, M. Pechal, J. Heinsoo, S. Storz, A. Blais, and A. Wallraff, Fast and unconditional all-microwave reset of a superconducting qubit, Phys. Rev. Lett. **121**, 060502 (2018).

[67] R. Acharya *et al.* (Google Quantum AI and Collaborators), Suppressing quantum errors by scaling a surface code logical qubit, Nature (London) **614**, 676 (2023).

[68] G. Kim, A. Butler, V. S. Ferreira, X. S. Zhang, A. Hadley, E. Kim, and O. Painter, Fast unconditional reset and leakage reduction of a tunable superconducting qubit via an engineered dissipative bath, Phys. Rev. Appl. **24**, 014013 (2025).

[69] M. McEwen *et al.*, Removing leakage-induced correlated errors in superconducting quantum error correction, Nat. Commun. **12**, 1761 (2021).